

The Delicate Bistability of CaMKII

P. J. Michalski*

Richard D. Berlin Center for Cell Analysis and Modeling, University of Connecticut Health Center,
Farmington, Connecticut

Michalski

CaMKII Activation and Dynamics

Submitted February 27, 2013, and accepted for publication June 25, 2013.

*Correspondence: michalski@uchc.edu

Supporting Text

Modeling Platforms

We used a custom Java program to run network free simulations of the system described above. A nearly identical program was described in (1). Briefly, CaMKII holoenzymes are stored as $N \times 1$ arrays, where N is the number of subunits in a holoenzyme, where each array element stores the state of an individual subunit. Each subunit could undergo one of the three types of reactions described above, with actual transition probabilities determined by the current state of the subunit and the state of its neighboring subunits. For inter-subunit phosphorylation, the i th subunit could phosphorylate the $(i + 1)$ th subunit, and the N th subunit could phosphorylate the 1st subunit. All simulations contained a total of 6000 subunits ($6000/N$ holoenzymes), which 1) produced sufficiently small deviation from the mean without becoming too computationally taxing and 2) is approximately the number of subunits present in the PSD ($200 \mu\text{M}$ CaMKII in a PSD of radius $0.5 \mu\text{m}$ and height 50 nm). For steady state measurements, the system was run for a time T to reach steady state (T depends on the actual system parameters), then run for an additional time T while data was recorded (≥ 100 time points), and steady state values are reported as the averages and standard deviations of these time points. For time dependent measurements, data from at least 5 simulations were used to obtain averages and standard deviations at each time point. We have previously shown that the system properties become independent of holoenzyme size when there are six or more subunits per holoenzyme (1), and unless noted otherwise we used hexameric holoenzymes in all of the results shown below.

Particle-based stochastic simulations are generally much slower than deterministic numerical simulations. Some results reported here required extensive parameter searches (notably the comparison to experimental results), and for these searches we used either of two deterministic models based on a dimer holoenzyme, which requires few enough species to be practically implemented in conventional modeling software. For dynamic simulations we used a Virtual Cell (2) model described previously (1), while steady state solutions were explored using a custom Mathematica code. In all cases, once appropriate parameter ranges were identified, we used the particle-based Java simulation to obtain the results presented here.

Each model was verified by simulating sub-systems which could be compared to analytic results, and verified against each other for more general cases. The Java program and the Mathematica code are available upon request. The VCell model “CaMKII Dimer v2.0” is publicly available under the username `pjmichal`.

Model Validation

We validated the dynamic properties of the model by comparing the model results to the classic experiments of De Koninck and Schulman (3), which demonstrated the frequency dependence of CaMKII autonomy. In these experiments, CaMKII immobilized in a flow chamber was exposed to pulses of ATP and varying amounts of calcium-saturated CaM, and CaMKII autonomy was measured as a function of pulse duration and frequency. Figure S2 compares the model outputs to

the experimental results. Figure S2(A) shows the autonomy generated by a continuous 6 second pulse as the concentration of CaM is varied. Under the experimental conditions maximal autonomy is 80% of the maximal Ca^{2+} /CaM-stimulated activity. Thus, for our simulation results, we multiply the fraction of autonomous subunits by 0.8 to obtain a fractional autonomous activity. Figure S2(B) shows the autonomy generated by one hundred, 200 ms pulses as a function of time for stimuli of different frequencies. Autonomy is generated more rapidly by higher frequencies. Figure S2(C) shows autonomy is a highly non-linear function of frequency. For the experiments in Fig. S2(C), CaMKII was exposed to pulses of varying duration, but the total number of pulses was varied in order to keep the total stimulus exposure constant at 6 seconds. The system response depends on both the pulse duration and frequency. For all of these experiments, the model results are in excellent qualitative and quantitative agreement with the experimental results. We conclude that the model accurately captures CaMKII dynamics.

We validated the equilibrium properties of the model by comparing the model results against data from Ref. (4). These experiments measured steady state CaMKII autonomy as a function of Ca^{2+} as both total CaMKII and total PP1 were varied. No autonomous activity was detected at $0.2 \mu\text{M}$ CaMKII and $2.5 \mu\text{M}$ PP1, which suggests that autonomy was below the detection threshold in this assay. We included this detection threshold by plotting our simulation results as

$$\frac{A}{A_{\max}} = \frac{E - E_{\text{th}}}{E_{\max} - E_{\text{th}}} \quad \text{for } E > E_{\text{th}}, \quad (1)$$

where A is the measured autonomy, E is the concentration of active kinase subunits, and E_{th} is the threshold kinase concentration below which any activity is indistinguishable from background, and A is normalized to the maximum autonomy under the given conditions. We assume that E_{th} depends on the concentration of CaMKII but not on any other variables. This gave three free parameters, one each for Figs. S3(A), (B), and (C), which we found by a direct least-squares fit. The agreement between the model and the experimental data is excellent. Notably, the model does not predict any regions of bistability for these concentrations, in agreement with the experimental data.

Cooperative Calmodulin Binding

Early studies of CaMKII activation concluded that CaM binds CaMKII in a non-cooperative manner (see, for example, Fig. 2b in Ref. (3), or Fig. 2a in Ref. (4)), and this is the mechanism included in the model used in the main text. However, there is recent evidence that CaM binds CaMKII cooperatively (5), with measured Hill coefficients ranging from 1.5 to 4.3 depending on various mutations to the regulatory domain. It is not known why such cooperativity was missed in earlier studies. It has been proposed (6, 7) that cooperativity arises because the regulatory domains of neighboring subunits pair up in the autoinhibited holoenzyme; CaM binding to one subunit disrupts this interaction, making the previously paired regulatory domain readily available for CaM binding. The actual mechanism must be more complex because a simple dimerization mechanism cannot account for Hill coefficients larger than 2, and may involve the interaction of neighboring subunit dimers.

In order to assess whether the possibility of CaM cooperativity could affect our conclusion that bistability is an insignificant component of CaMKII physiology, we studied the effect of cooperative CaM binding using a dimer model for the CaMKII holoenzyme. Such a scheme will not reproduce the full extent of observed cooperativity, but will indicate how and to what extent activation curves will change as cooperativity is turned on. Cooperativity can be implemented by varying either the on or the off rates; here we choose to only vary the on rates. To determine how those rates should change, it is useful to consider CaM binding to CaMKII in the absence of phosphorylation reactions (which is realized in practice by making the mutations T286A/T305A/T306A). In this case each subunit is in one of two states, either inactive or CaM-bound, and the dimer can be in one of four possible configurations, denoted as M_{00} , M_{01} , M_{10} , and M_{11} , where the two indices refer to each subunit, and a 0 indicates an inactive subunit and a 1 indicates a CaM-bound subunit. The reaction scheme for this system is shown in Fig. S18, where CaM binding to the completely inhibited dimer occurs with an on-rate of βk_+ , and CaM binding to the partially active dimer occurs with an on-rate of αk_+ , and $\alpha = \beta = 1$ corresponds to the non-cooperative limit. The fraction of active subunits, A , is given by

$$A = \frac{M_{10} + M_{01} + M_{11}}{M_{\text{tot}}}, \quad (2)$$

where $M_{\text{tot}} = M_{00} + M_{10} + M_{01} + M_{11}$ is the total concentration of dimers. We can write this in terms of the total concentration of calcium-saturated CaM, C , as

$$A = \frac{2\alpha\beta \left(\frac{C}{K_0}\right) \left(\frac{1}{\alpha} + \frac{C}{K_0}\right)}{1 + 2\beta \left(\frac{C}{K_0}\right) + \alpha\beta \left(\frac{C}{K_0}\right)^2}, \quad (3)$$

where $K_0 = k_-/k_+$ is the non-cooperative dissociation constant. The effective dissociation constant, K_{eff} , is the CaM concentration giving 50% activity, and is given by

$$K_{\text{eff}} = \frac{K_0}{\sqrt{\alpha\beta}}. \quad (4)$$

In order to have a well-defined dissociation constant in the infinitely cooperatively limit, $\alpha \rightarrow \infty$, we must simultaneously take $\beta \rightarrow 0$, and we therefore set $\beta = 1/\alpha$.

In the full model, we assume that the dimerization of regulatory domains is disrupted by modifications which activate the kinase (either CaM-binding or T286 phosphorylation), but not by those which leave the kinase inactive (basal autophosphorylation on T305). Thus, if both subunits of a dimer are inactive, then the on-rate to both is reduced by a factor $1/\alpha$, while if either subunit is active, then the on-rate to both is increased by a factor α . The non-cooperative model is recovered by letting $\alpha = 1$. All other reactions remain as described in the main text. This scheme was implemented in a VCell model, “Dimer_CooperativeCaMBinding02”, which is publicly available under the username `pjmichal`. We ran and analyzed over 31000 simulations of this model in order to fully explore the relevant parameter space.

To begin, we verified that the dimer model recapitulates the activation curves of the hexamer discussed in the main text. We found that the dimer required a larger concentration of total

subunits in order to saturate the phosphatase and allow for any regions of bistability. We therefore increased the concentration of CaMKII subunits from 200 μM to 2000 μM . We used 100 μM CaM and the fast set of autophosphorylation rates, $r_1 = 10 \text{ s}^{-1}$. These conditions provided the lowest thresholds to activation (but still well above basal calcium levels) and give the best chance to observe cooperativity-induced changes which might alter the behavior at basal calcium levels. The non-cooperative activation curves for these conditions are shown in Fig. S19 and do indeed recapitulate the activation curves of the hexamer. As phosphatase activity increases, the activation curves go from laser-like to step-like (with narrow regions of bistability) and finally to Hill-like at very high phosphatase activity. Even at these high CaM concentrations and fast autophosphorylation rates, the regions of bistability occur at calcium concentration five times higher than basal levels.

When cooperativity is turned on we find no significant qualitative differences in the types of activation curves; that is, curves are always either laser-like, step-like (with narrow regions of bistability far above basal calcium), or Hill-like. However, for a given parameter set, cooperativity can convert one type of curve into another. We found five types of behavior:

- 1) Laser-like curve becomes Hill-like.
- 2) Step-like curve becomes laser-like.
- 3) Step-like curve remains step-like.
- 4) Hill-like curves becomes step-like.
- 5) Hill-like curve remains Hill-like but with a larger Hill coefficient.

These five behaviors are illustrated in Fig. S20, where we show how several curves from Fig. S19 evolve as α is increased in powers of 10 from 1 to 1000. (In each case we continued to increase α in powers of 10 up to 10^6 in order to verify a limiting behavior had been reached.) Importantly, even at these high CaM concentrations and fast autophosphorylation rates, the regions of bistability occur at calcium concentrations five times higher than basal levels. Additionally, as in the non-cooperative CaM case analyzed in the main text of this paper, the range of Ca^{2+} concentrations that display bistability are so small as to be physiologically negligible. We conclude that cooperative CaM binding does not change the qualitative behavior of CaMKII activation curves.

This conclusion is not surprising because there are already two mechanisms of cooperativity at work in CaMKII activation, namely, cooperative calcium binding to CaM and cooperative autophosphorylation on T286. These cooperative mechanism are sufficient to produce very large Hill coefficients and step-like activation curves, which are generally the main features associated with cooperative activation. Adding a third source of cooperativity to such a strongly cooperative system is unlikely to have a significant effect, as verified by the results above.

Supporting Tables

Parameter	Description	Value	Reference
K_0	Dissociation constant for Ca^{2+} binding CaM_0	$20 \mu\text{M}$	(8)
K_1	Dissociation constant for Ca^{2+} binding CaM_1	$0.57 \mu\text{M}$	(8)
K_2	Dissociation constant for Ca^{2+} binding CaM_2	$100 \mu\text{M}$	(8)
K_3	Dissociation constant for Ca^{2+} binding CaM_3	$5 \mu\text{M}$	(8)
$k_{\text{off},u}^{(1)}$	CaM_4 , D_{uu} direct dissociation rate	2 s^{-1}	(9, 10)
$k_{\text{off},u}^{(2)}$	CaM_4 , D_{uu} maximum Ca^{2+} -mediated dissociation rate	4.3 s^{-1}	Fit to data in Ref. (9)
$K_{\text{Ca},u}$	EC_{50} for CaM_4 , D_{uu} Ca^{2+} -mediated dissociation	$0.94 \mu\text{M}$	Fit to data in Ref. (9)
$k_{\text{on},u}$	CaM_4 , D_{uu} association rate	$30 \mu\text{M}^{-1} \text{ s}^{-1}$	Based on $k_{\text{off},u}$ and $K_D \approx 66.7 \text{ nM}$
$k_{\text{off},p}^{(1)}$	CaM_4 , D_{pu} direct dissociation rate	0.001 s^{-1}	(9)
$k_{\text{off},p}^{(2)}$	CaM_4 , D_{pu} maximum Ca^{2+} -mediated dissociation rate	0.08 s^{-1}	(9)
$K_{\text{Ca},p}$	EC_{50} for CaM_4 , D_{pu} Ca^{2+} -mediated dissociation	$0.19 \mu\text{M}$	(9)
$k_{\text{on},p}$	CaM_4 , D_{pu} association rate	$10 \mu\text{M}^{-1} \text{ s}^{-1}$	(9)
r_1	C_u -mediated T286 phosphorylation rate	1.0 s^{-1} or 10 s^{-1}	Order of magnitude estimate.
r_2	C_p -mediated T286 phosphorylation rate	r_1	Based on activity towards exogenous substrates.
r_3	D_{pu} -mediated T286 phosphorylation rate	$0.8r_1$	Based on autonomous activity towards exogenous substrates.
r_4	D_{pp} -mediated T286 phosphorylation rate	r_3	D_{pp} and D_{pu} have same activity towards exogenous substrates (11).
r_{305}	D_{pu} T305 autophosphorylation rate	10 s^{-1}	Order of magnitude estimate.
r_b	D_{uu} T305 basal autophosphorylation rate	$5 \times 10^{-4} \text{ s}^{-1}$	(12)

Table S1: Model parameters for Ca^{2+} -CaM binding and CaMKII autophosphorylation.

Parameter	Description	Value	Reference
k_{cat}	PP1-mediated CaMKII dephosphorylation rate.	1.72 s^{-1}	(4)
K_m	PP1-mediated CaMKII dephosphorylation Michaelis-Menton constant.	$11 \mu\text{M}$	(4)
$k_{\text{on,PP1}}$	I1, PP1 association rate	$500 \mu\text{M}^{-1} \text{ s}^{-1}$	(13)
$k_{\text{off,PP1}}$	I1, PP1 dissociation rate	0.1 s^{-1}	(13)
$k_{\text{CaN}}^{(0)}$	Basal CaN activity	0.1 s^{-1}	(14)
k_{CaN}	Maximum Ca/CaM stimulated CaN activity	18 s^{-1}	(14)
K_{CaN}	CaN activity EC_{50}	$0.053 \mu\text{M}$	(14)
n_{CaN}	CaN activity Hill coefficient	3	(14)
$k_{\text{PKA}}^{(0)}$	Basal PKA activity	0.0036 s^{-1}	(14)
k_{PKA}	Maximum Ca/CaM stimulated PKA activity	100 s^{-1}	(14)
K_{PKA}	PKA activity EC_{50}	$0.11 \mu\text{M}$	(14)
n_{PKA}	PKA activity Hill coefficient	8	(14)

Table S2: Model parameters for PP1 activity.

Supporting Figures

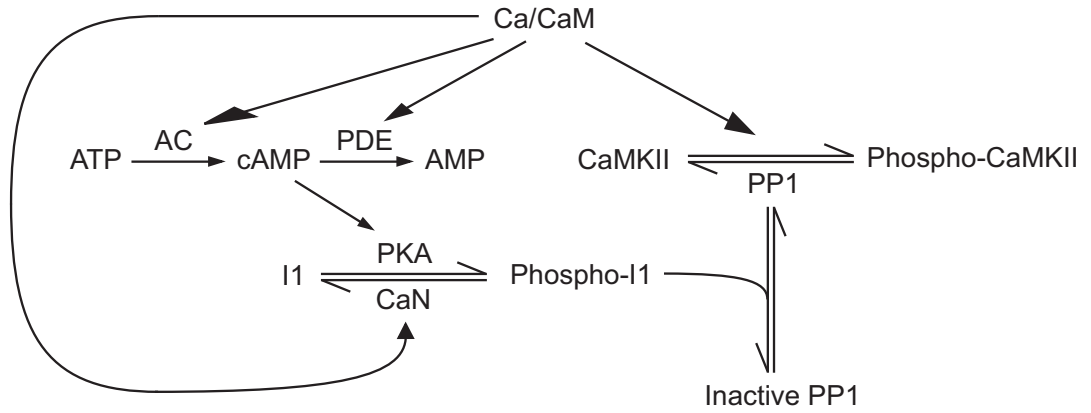


Figure S1: **PP1 regulation.** (A) A schematic reaction diagram demonstrating two mechanisms of Ca/CaM-dependent PP1 regulation. CaM directly activates CaN, which increases PP1 activity by dephosphorylating I1. CaM also acts indirectly through the cAMP pathway by controlling the activity of CaM-dependent ACs and PDEs. This pathway decreases PP1 activity through PKA-dependent phosphorylation of I1.

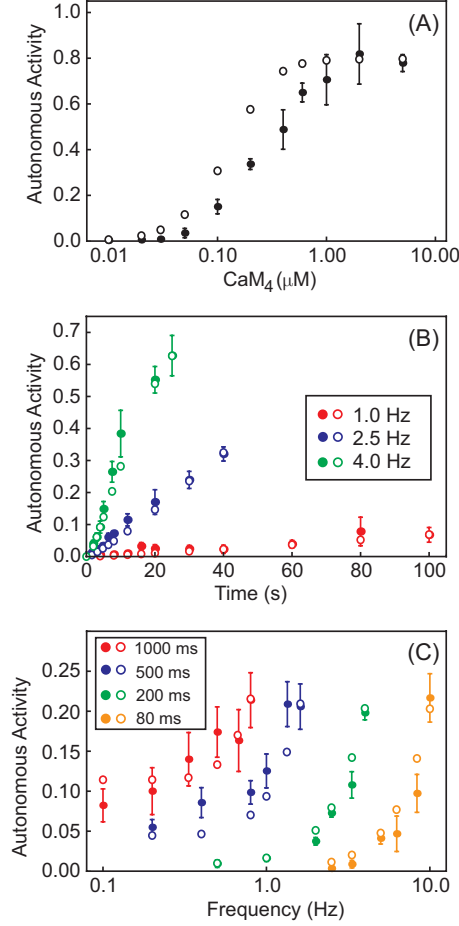


Figure S2: **Validation of the model dynamics.** The model is used to reproduce the results of Ref. (3). Experimental results are labeled by closed circles and error bars, simulation results are labeled with open circles. Autonomous activity is defined relative to the maximum $\text{Ca}^{2+}/\text{CaM}$ -stimulated activity of an identically treated sample. (A) CaMKII autonomy as a function of saturated CaM. CaMKII was exposed to a continuous 6-second stimulation with varying concentrations of saturated CaM. The model reproduces the experimental Hill coefficient but slightly underestimates the measured EC_{50} . (B) CaMKII autonomy as a function of time. CaMKII was exposed to one hundred, 200 ms pulses of $0.1 \mu\text{M}$ CaM₄ at one of three different frequencies, as indicated in the figure legend. (C) CaMKII autonomy as a function of frequency. CaMKII was exposed to $0.1 \mu\text{M}$ CaM₄ pulses of different durations and frequencies, with the total number of pulses adjusted to keep total exposure time at 6 seconds. The curves are color coded according to pulse duration, as indicated in the figure legend. Parameters: $\text{CaMKII}_{\text{tot}} = 0.005 \mu\text{M}$, $k_{\text{on},u} = 4.0 \mu\text{M}^{-1} \text{s}^{-1}$, $k_{\text{off},u} = 0.66 \text{s}^{-1}$, $r_1 = 1.0 \text{s}^{-1}$.

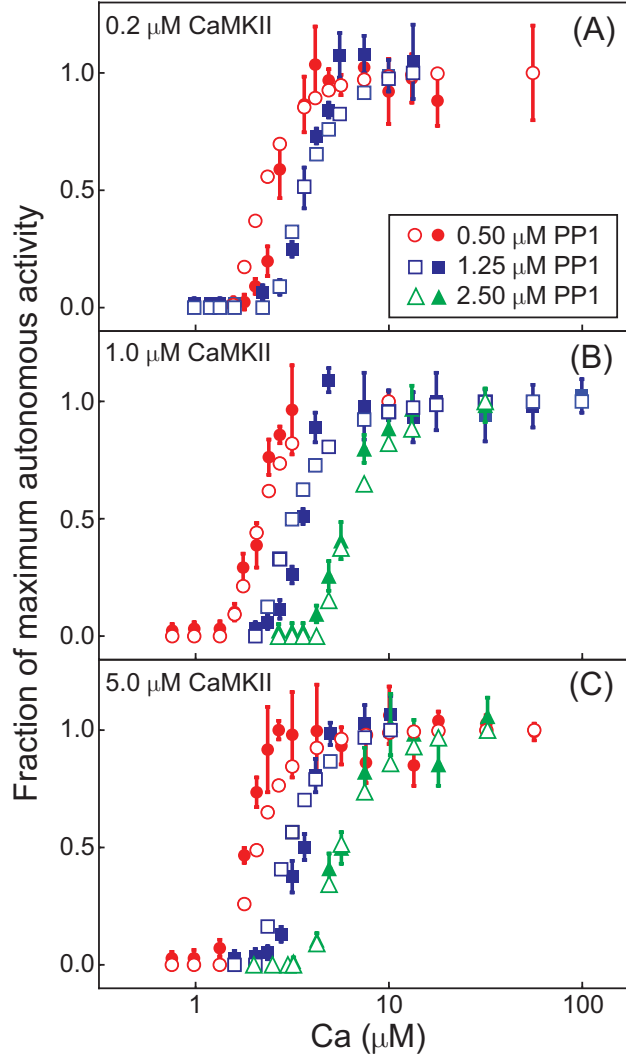


Figure S3: **Validation of steady state properties.** The model is used to reproduce the results of Ref. (4). Experimental results are labeled with closed symbols and error bars, model results are labeled with open symbols. Each plot shows the fraction of maximal autonomous activity as a function of Ca^{2+} as the total concentrations of CaMKII and PP1 are varied. (A) $0.2 \mu\text{M}$ CaMKII, (B) $1.0 \mu\text{M}$ CaMKII, (C) $5 \mu\text{M}$ CaMKII. The curves are color coded according to the concentration of PP1, as indicated in the legend. The fitted values of E_{th} were (A) $0.05 \mu\text{M}$, (B) $0.15 \mu\text{M}$, and (C) $0.75 \mu\text{M}$. Other parameters: $\text{CaM}_{\text{tot}} = 50 \mu\text{M}$, $r_1 = 1 \text{ s}^{-1}$, $r_3 = r_4 = 0$ (according to (4)), $K_0 = 10 \mu\text{M}$, $K_1 = 0.1 \mu\text{M}$, $k_{\text{on},u} = 3 \mu\text{M}^{-1} \text{ s}^{-1}$, and $k_{\text{on},p} = 0.3 \mu\text{M}^{-1} \text{ s}^{-1}$.

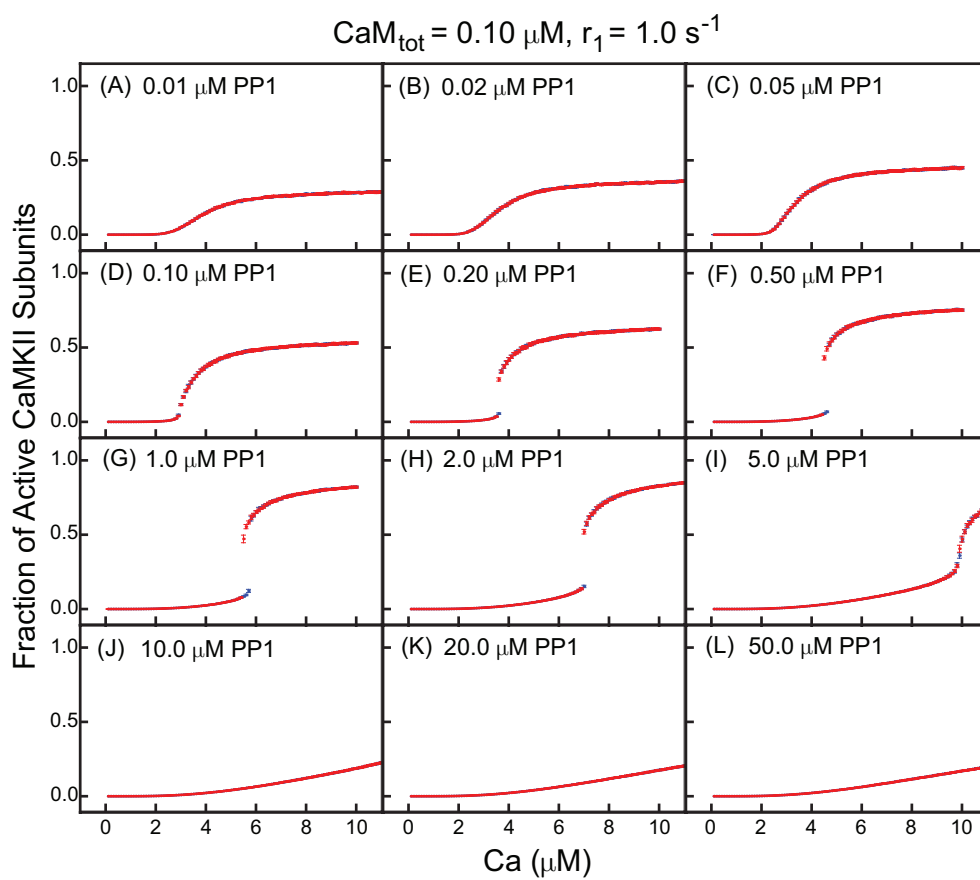


Figure S4: **Steady state activity curves.** Same as Fig. 6 but for $\text{CaM}_{\text{tot}} = 0.1 \mu\text{M}$ and $r_1 = 1 \text{ s}^{-1}$.

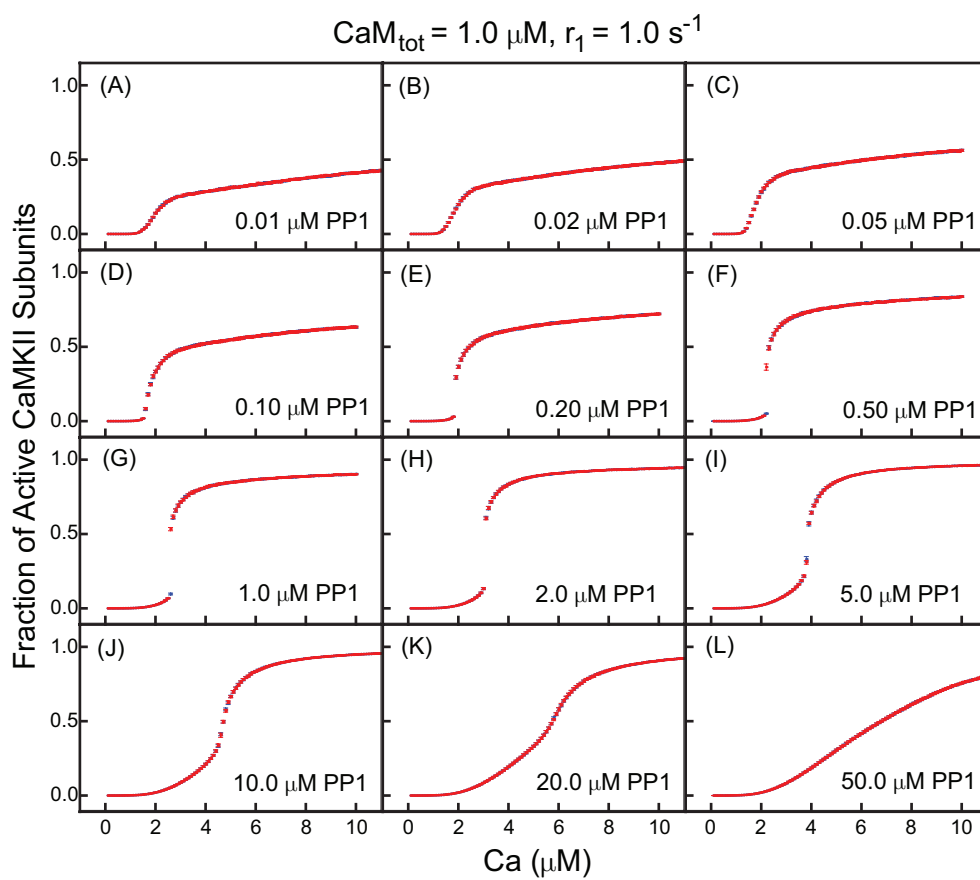


Figure S5: **Steady state activity curves.** Same as Fig. 6 but for $\text{CaM}_{\text{tot}} = 1 \mu\text{M}$ and $r_1 = 1 \text{ s}^{-1}$.

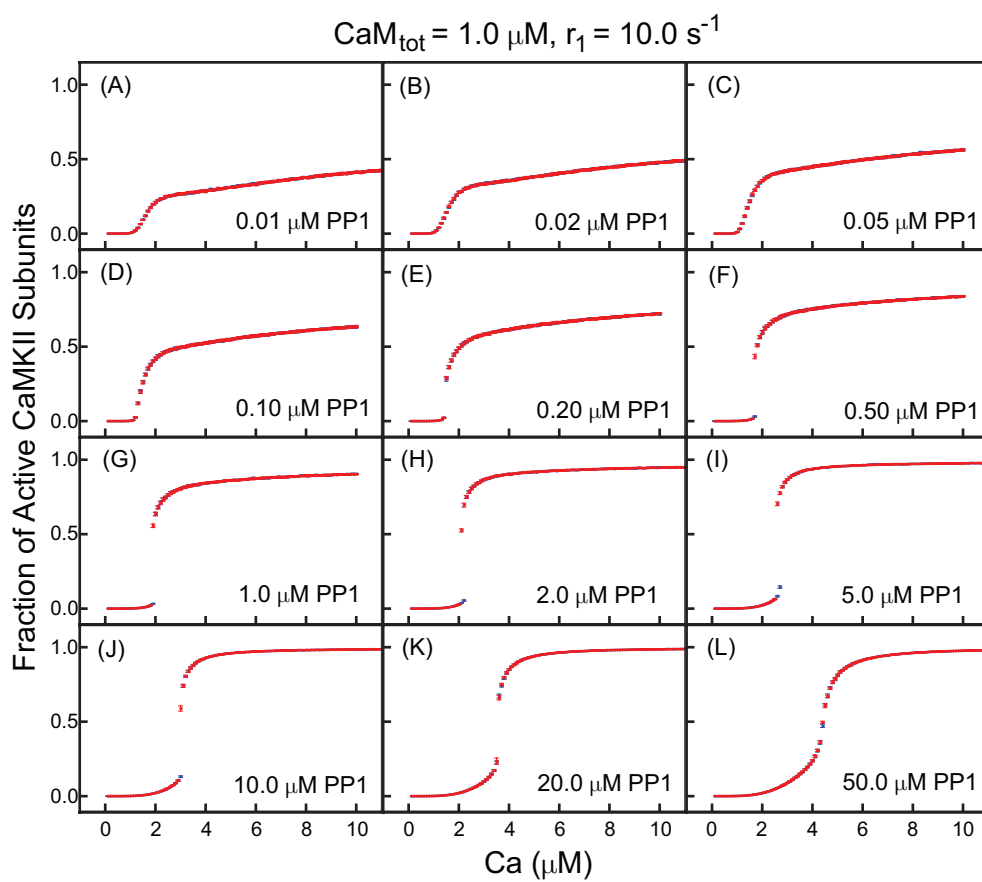


Figure S6: **Steady state activity curves.** Same as Fig. 6 but for $\text{CaM}_{\text{tot}} = 1 \mu\text{M}$ and $r_1 = 10 \text{ s}^{-1}$.

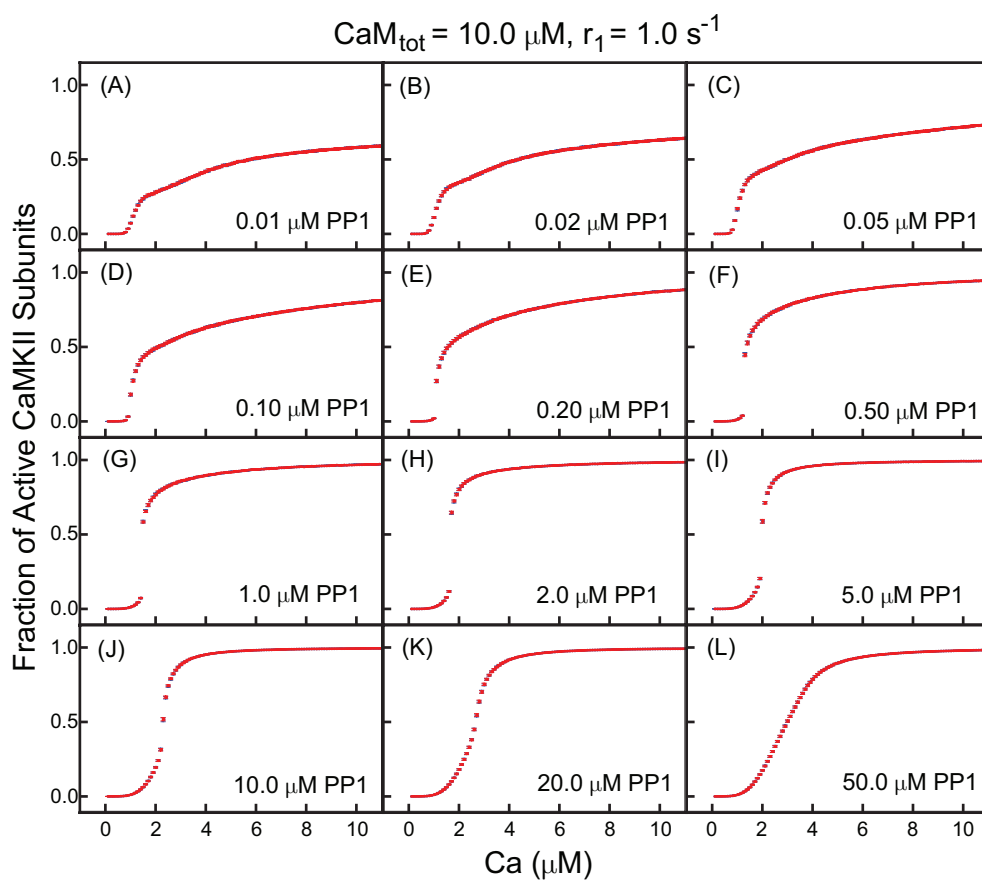


Figure S7: **Steady state activity curves.** Same as Fig. 6 but for $\text{CaM}_{\text{tot}} = 10 \mu\text{M}$ and $r_1 = 1 \text{ s}^{-1}$.

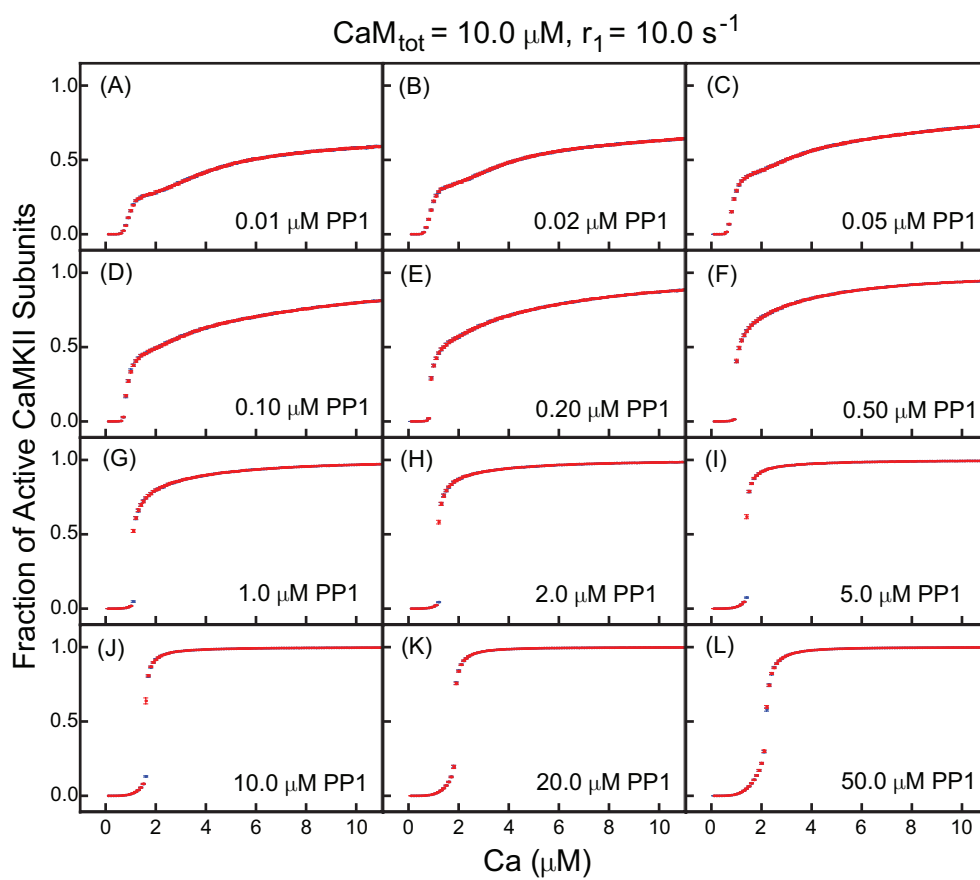


Figure S8: **Steady state activity curves.** Same as Fig. 6 but for $\text{CaM}_{\text{tot}} = 10 \mu\text{M}$ and $r_1 = 10 \text{ s}^{-1}$.

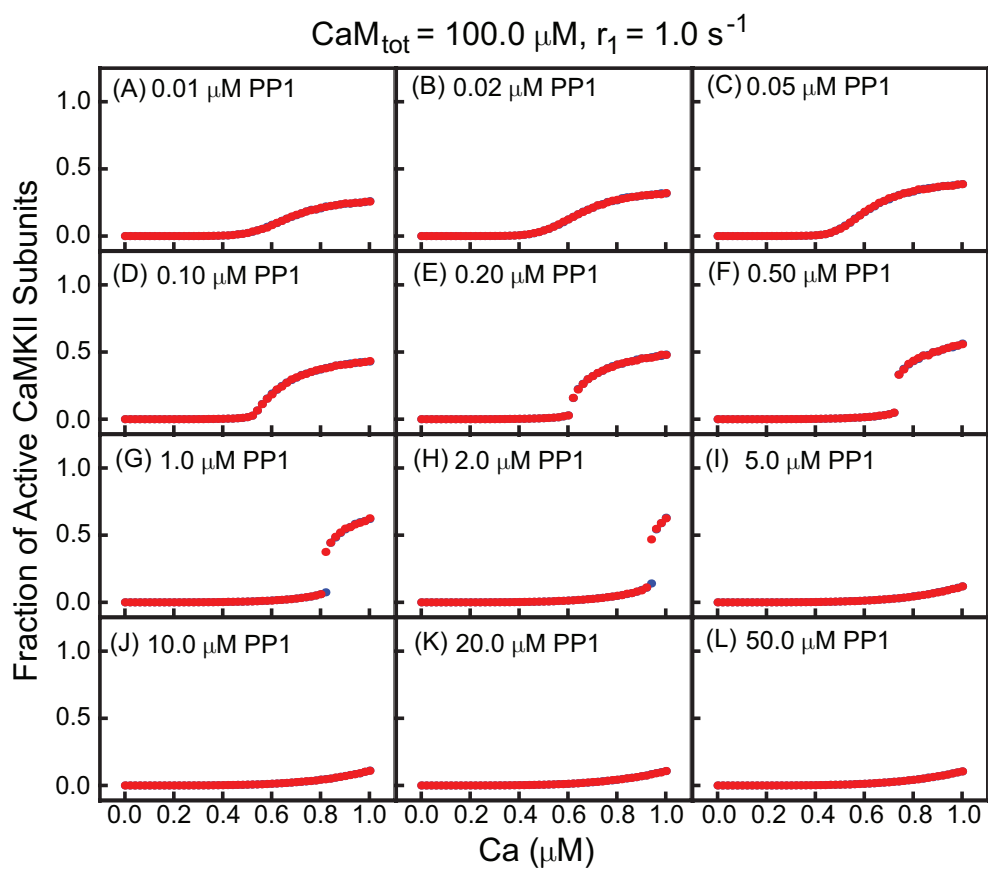


Figure S9: **Steady state activity curves.** Same as Fig. 6 but for $\text{CaM}_{\text{tot}} = 100 \mu\text{M}$ and $r_1 = 1 \text{ s}^{-1}$. Note that the x-axis is expanded compared to Fig. 6, to show the region near the origin.

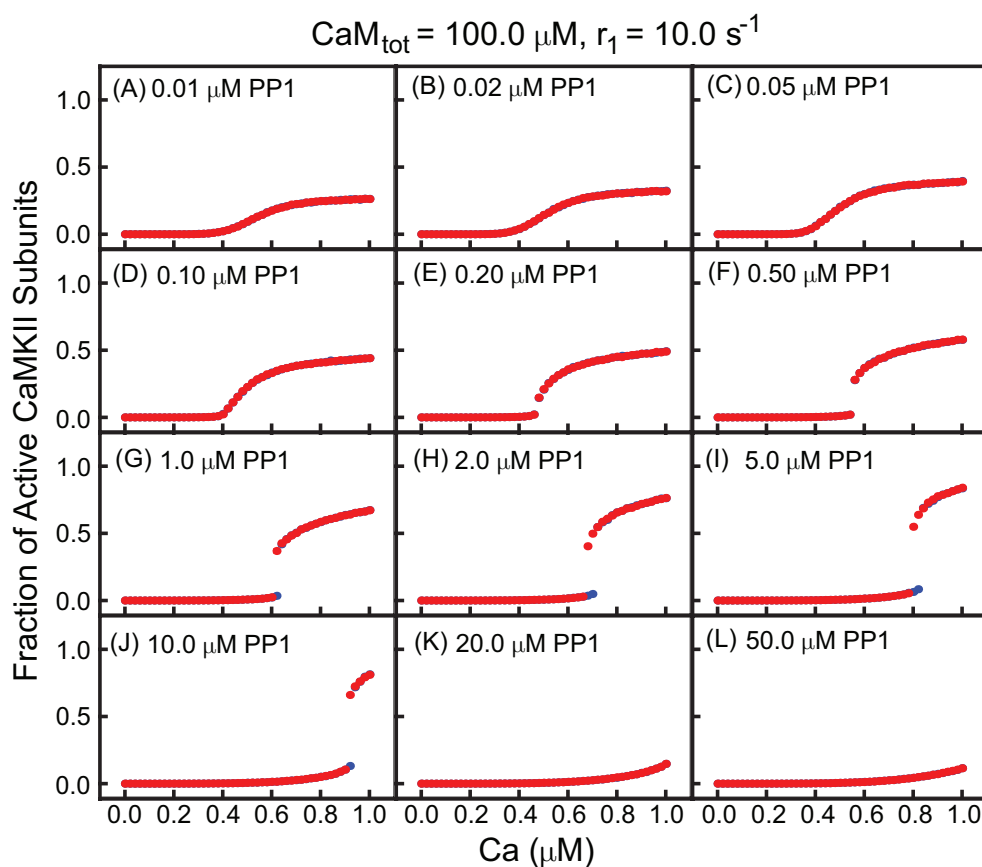


Figure S10: **Steady state activity curves.** Same as Fig. 6 but for $\text{CaM}_{\text{tot}} = 100 \mu\text{M}$ and $r_1 = 10 \text{ s}^{-1}$. Note that the x-axis is expanded compared to Fig. 6, to show the region near the origin.

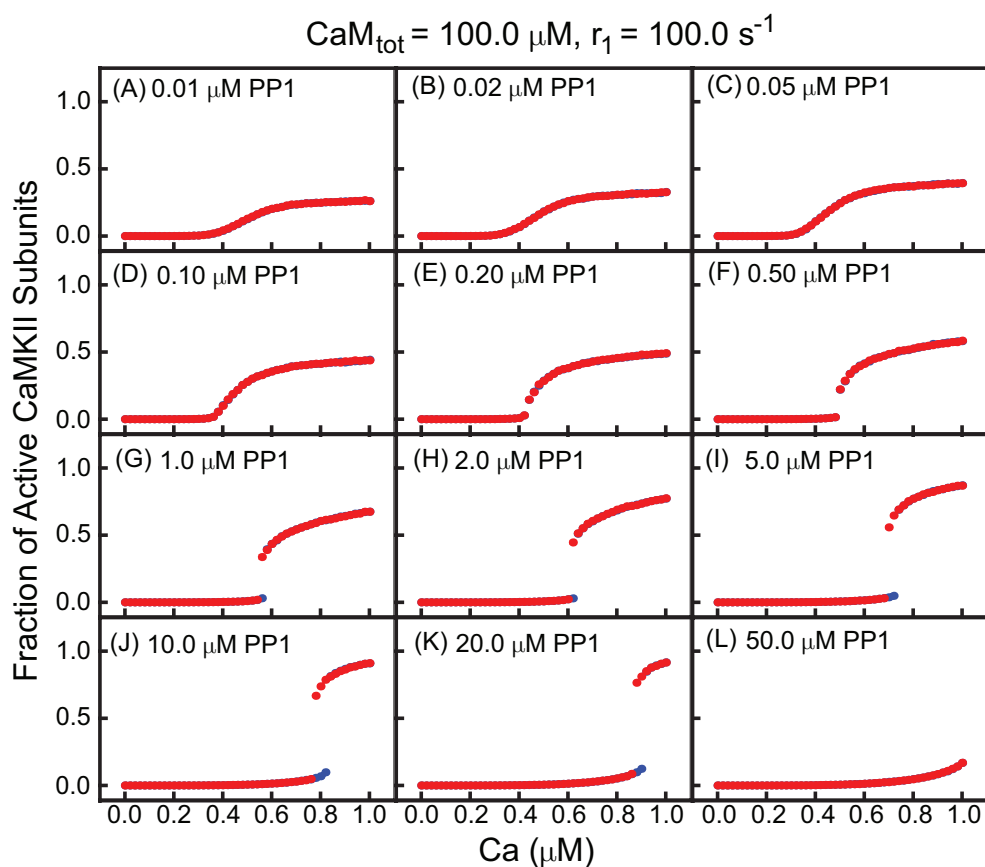


Figure S11: **Steady state activity curves.** Same as Fig. 6 but for $\text{CaM}_{\text{tot}} = 100 \mu\text{M}$ and $r_1 = 100 \text{ s}^{-1}$. Note that the x-axis is expanded compared to Fig. 6, to show the region near the origin.

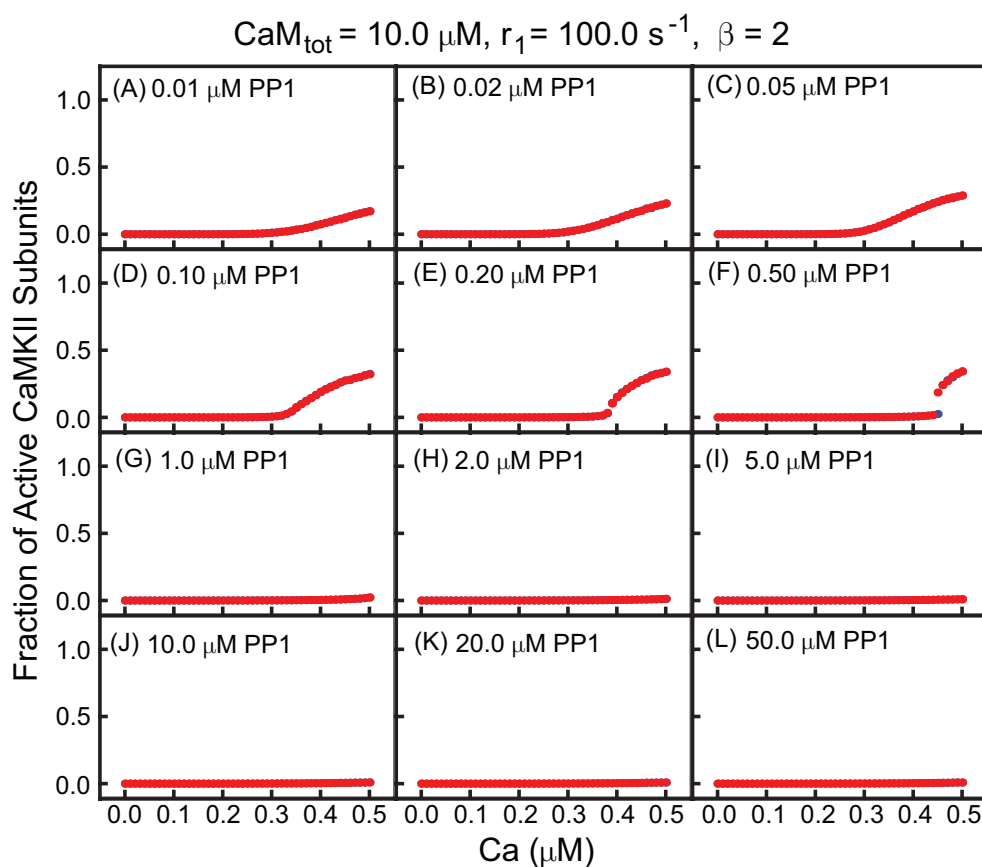


Figure S12: **Steady state activity curves with increased calcium-CaM affinity.** Same as Fig. 6 but for $\text{CaM}_{\text{tot}} = 10 \mu\text{M}$, $r_1 = 100 \text{ s}^{-1}$, and $\beta = 2$. Note that the x-axis is expanded compared to Fig. 6, to show the region near the origin.

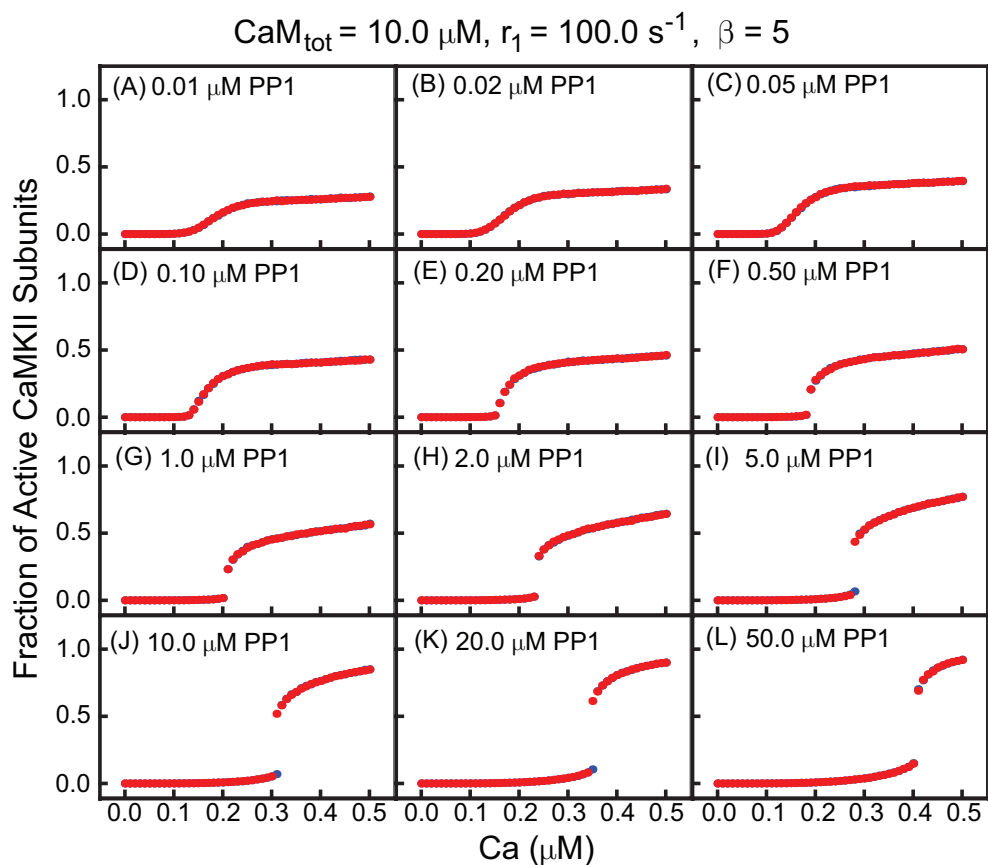


Figure S13: **Steady state activity curves with increased calcium-CaM affinity.** Same as Fig. 6 but for $\text{CaM}_{\text{tot}} = 10 \mu\text{M}$, $r_1 = 100 \text{ s}^{-1}$, and $\beta = 5$. Note that the x-axis is expanded compared to Fig. 6, to show the region near the origin.

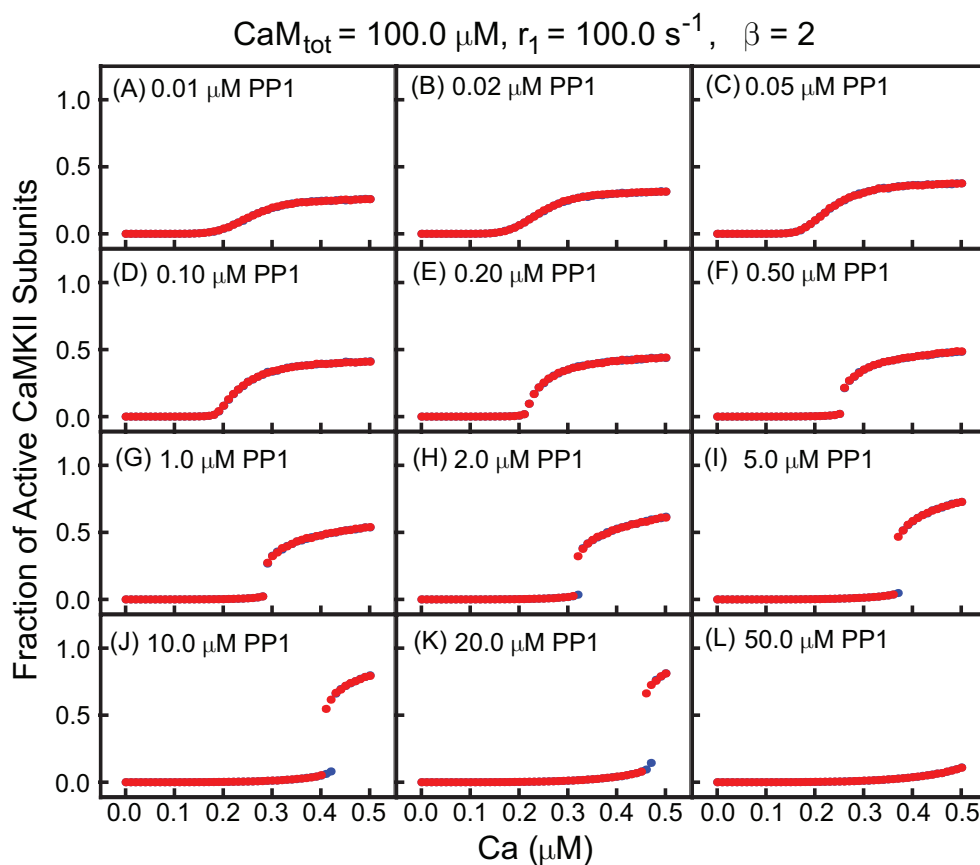


Figure S14: **Steady state activity curves with increased calcium-CaM affinity.** Same as Fig. 6 but for $\text{CaM}_{\text{tot}} = 100 \mu\text{M}$, $r_1 = 100 \text{ s}^{-1}$, and $\beta = 2$. Note that the x-axis is expanded compared to Fig. 6, to show the region near the origin.

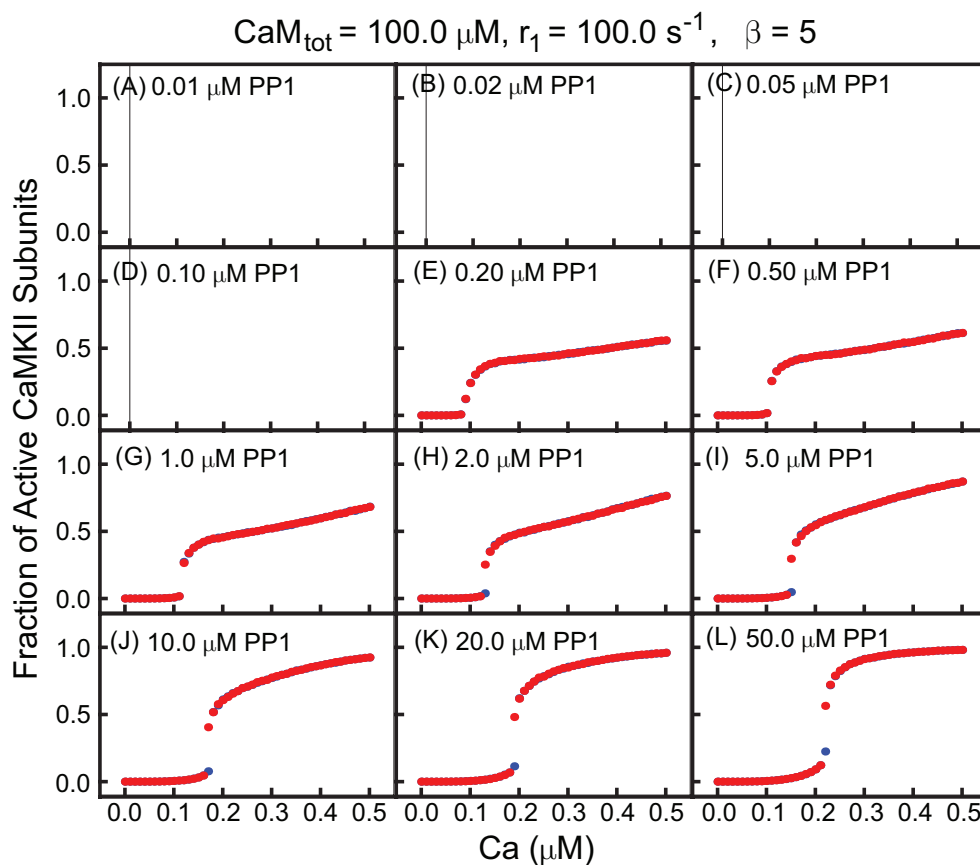


Figure S15: **Steady state activity curves with increased calcium-CaM affinity.** Same as Fig. 6 but for $\text{CaM}_{\text{tot}} = 100 \mu\text{M}$, $r_1 = 100 \text{ s}^{-1}$, and $\beta = 5$. Note that the x-axis is expanded compared to Fig. 6, to show the region near the origin.

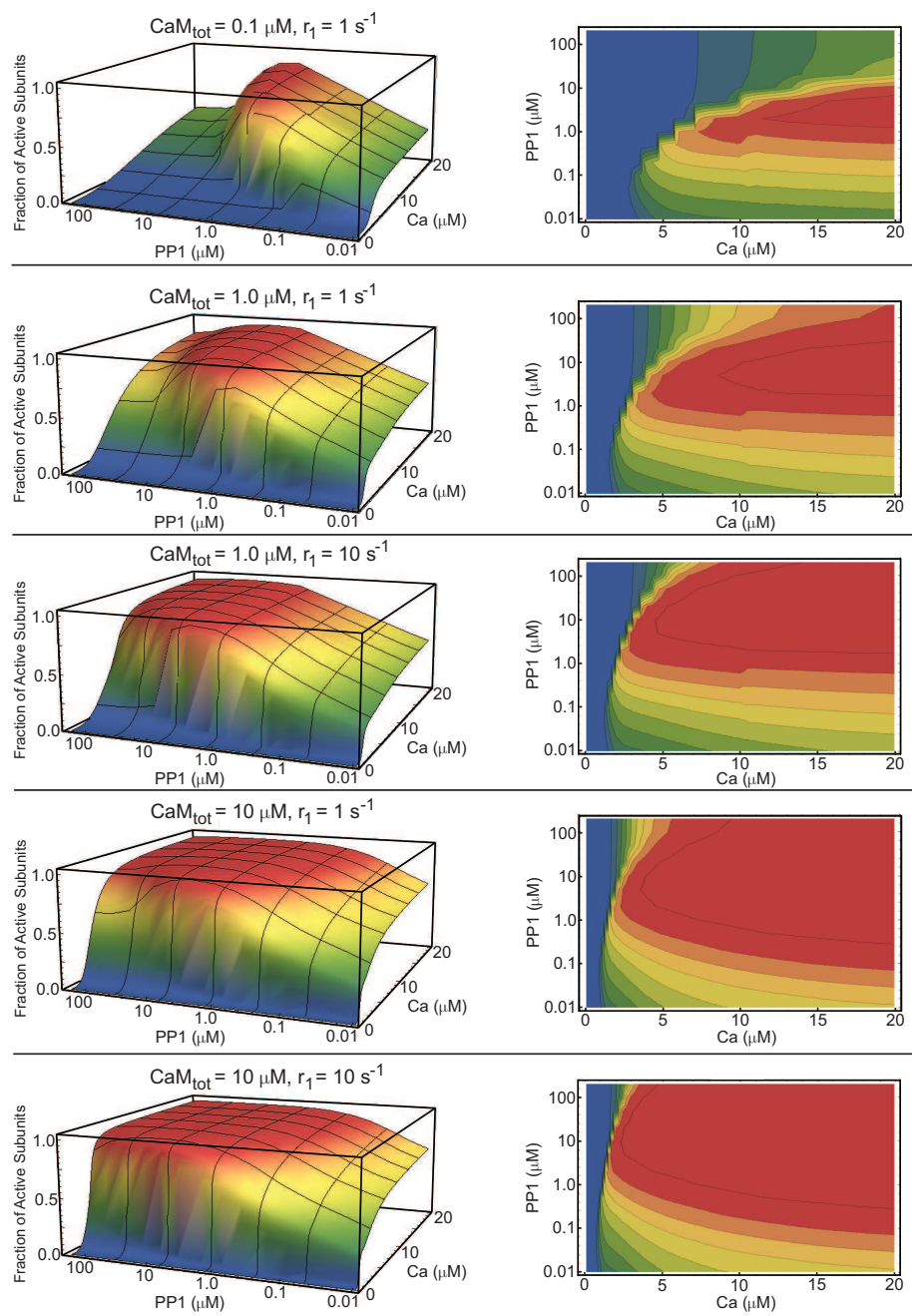


Figure S16: **CaMKII activity phase diagrams.** Same as Fig. 7, but for the activity curves shown in Figs. S4-S8.

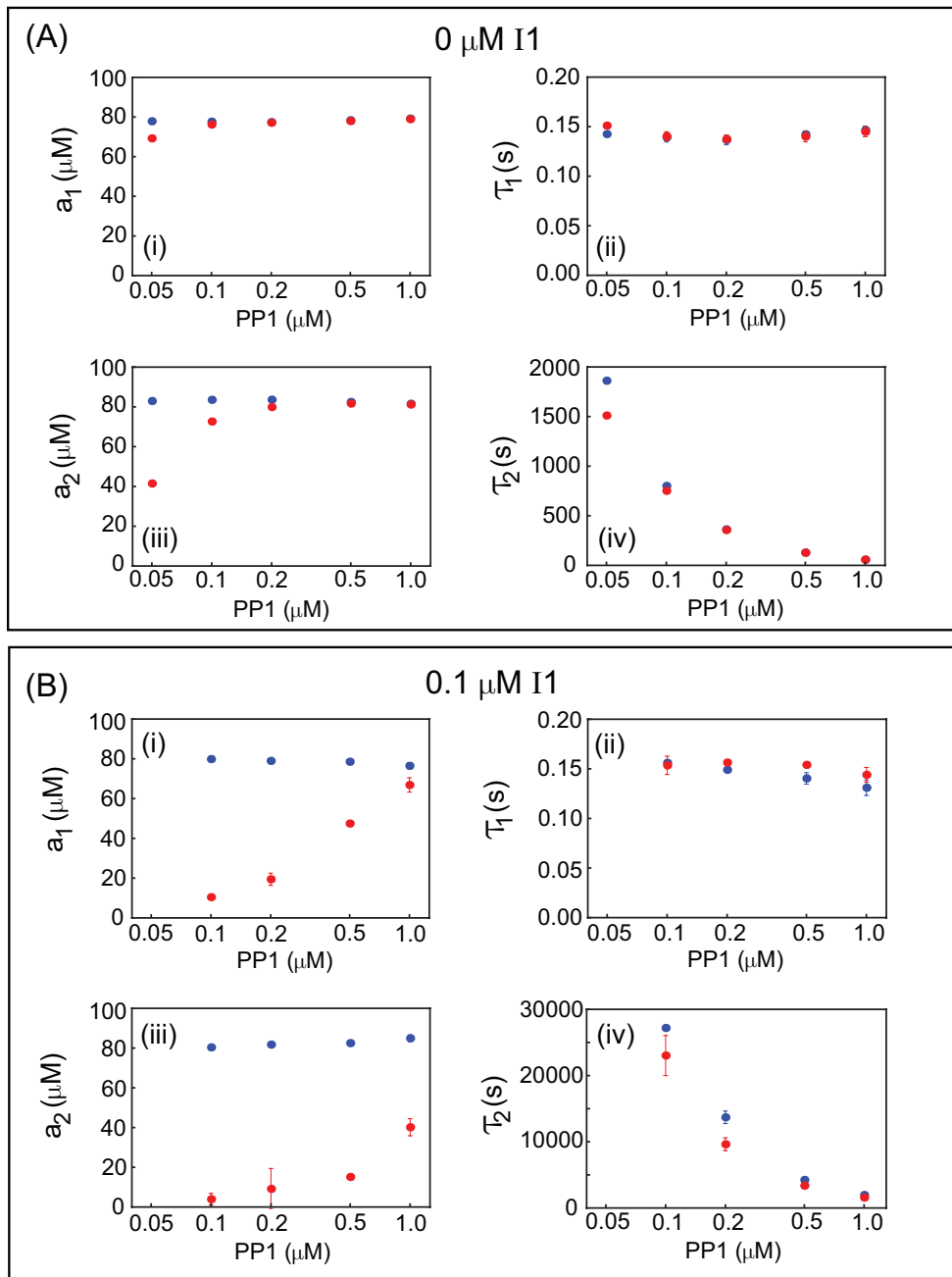


Figure S17: **Characterization of response to LTP protocols.** Same as Fig. 10, but for other values of $I_{1\text{tot}}$.

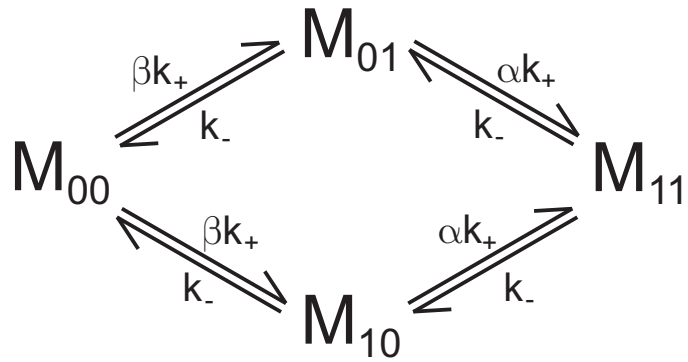


Figure S18: **Reaction scheme for dimer holoenzyme in absence of autophosphorylation.** The dimer holoenzyme can be described by four states depending on which subunit is inactive (0) and which is CaM-bound (1). The cooperative model considered in the Supporting Text assumes that all cooperativity arises from changes in the on-rate. CaM binding to the fully inhibited dimer occurs with an on-rate βk_+ , while CaM binding to the partially active dimer occurs with an on-rate of αk_+ . The non-cooperative limit occurs when $\alpha = \beta = 1$. In order to ensure a finite effective dissociation constant in the fully cooperative limit, $\alpha \rightarrow \infty$, we set $\beta = 1/\alpha$. See the Supporting Text for details.

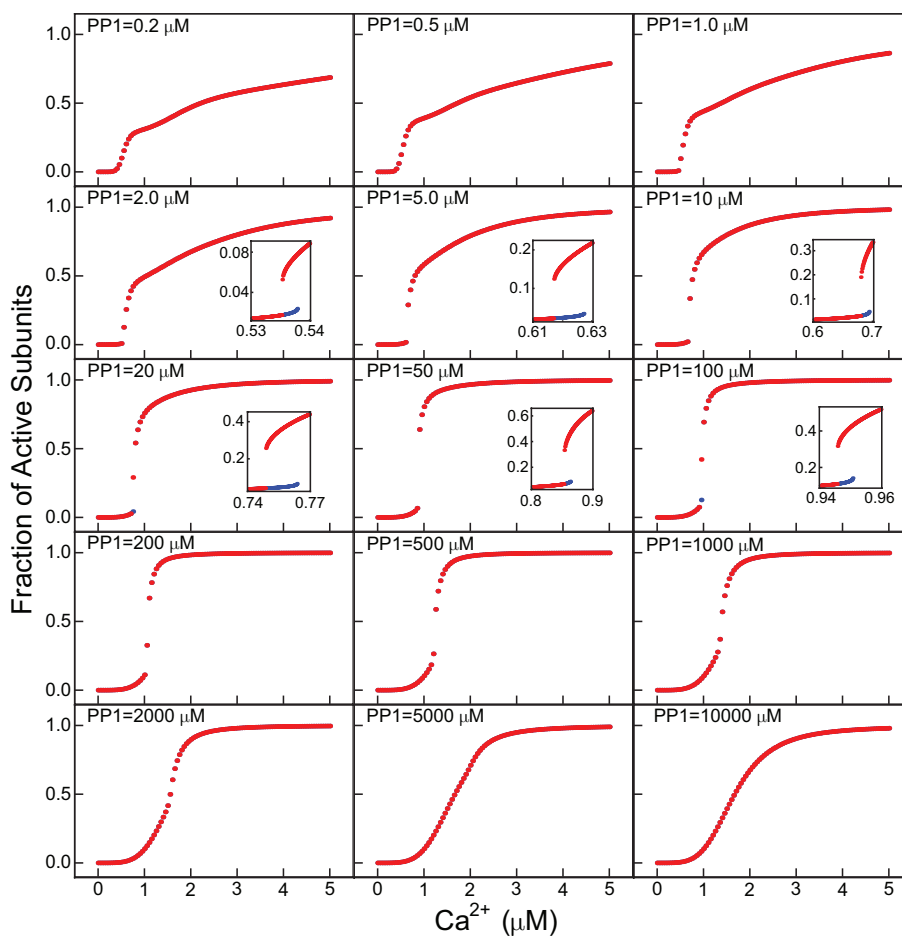


Figure S19: **Steady-state activation curves for the non-cooperative dimer holoenzyme.** CaMKII steady-state activation is plotted as a function of calcium for many values of PP1. A comparison of this figure with Fig. 6 shows that the dimer model is able to recapitulate the full range of behaviors seen in the hexamer. Blue data points are obtained as calcium is incremented from low to high values; red data points are obtained as calcium is decremented from high to low values. The insets show tiny regions of bistability which characterize step-like activation curves. Results obtained with standard parameters and the fast set of autophosphorylation rates ($r_1 = 10 \text{ s}^{-1}$, etc), while $\text{CaMKII} = 200 \text{ } \mu\text{M}$ and $\text{CaM} = 100 \text{ } \mu\text{M}$ for reasons discussed in the supporting text.

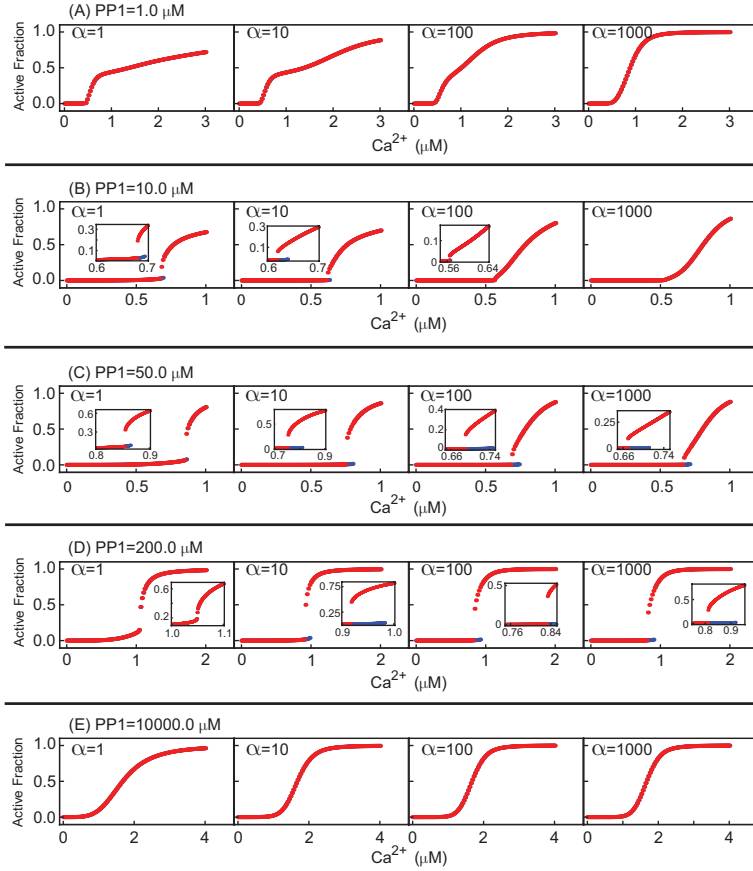


Figure S20: **The effect of cooperative CaM binding on steady state CaMKII activation curves.** These examples illustrate the full range of possible changes which occur as cooperativity is increased. The left-most curve in each row reproduces a non-cooperative curve from Fig. S19, while the other three curves show the effect of increasing cooperativity. Cooperativity is turned on by increasing α in powers of 10 up to 1000. (We continued this progression up to $\alpha = 10^6$ to verify a limiting behavior was attained at $\alpha = 1000$.) (A) Increasing cooperativity converts a laser-like activation curve to a Hill-like activation curve. (B) Increasing cooperativity converts a step-like activation with a narrow region of bistability into a laser-like activation. (C) Increasing cooperativity modifies the exact shape of the step-like activation curve but does not eliminate the narrow region of bistability. (D) Increasing cooperativity converts a very steep Hill-like curve into a step-like curve with a narrow region of bistability. (E) Increasing cooperativity increases the effective Hill coefficient of a Hill-like activation curve. Insets show expanded views of the regions of bistability, except the first inset in (D), which shows that no bistability is evident when calcium is incremented in steps of 1 nM. Blue curves: calcium incremented from low to high values. Red curves: calcium incremented from high to low values. All parameters as in Fig. S19.

References

1. Michalski, P. J., and L. M. Loew, 2012. CaMKII activation and dynamics are independent of the holoenzyme structure: an infinite subunit holoenzyme approximation. *Phys. Biol.* 9:036010.
2. Slepchenko, B. M., J. C. Schaff, I. Macara, and L. M. Loew, 2003. Quantitative cell biology with the Virtual Cell. *Trends Cell Biol.* 13:570 – 576.
3. De Koninck, P., and H. Schulman, 1998. Sensitivity of CaM kinase II to the frequency of Ca^{2+} oscillations. *Science* 279:227 – 230.
4. Bradshaw, J. M., Y. Kubota, T. Meyer, and H. Schulman, 2003. An ultrasensitive Ca^{2+} /calmodulin-dependent protein kinase II-protein phosphatase 1 switch facilitates specificity in postsynaptic calcium signaling. *PNAS* 100:10512 – 10517.
5. Chao, L. H., P. Pellicena, S. Deindl, L. A. Barclay, H. Schulman, and J. Kuriyan, 2010. Intersubunit capture of regulatory segments is a component of cooperative CaMKII activation. *Nat. Struct. Mol. Biol.* 17:264 – 272.
6. Rosenberg, O. S., S. Deindl, R.-J. Sung, A. C. Nairn, and J. Kuriyan, 2005. Structure of the autoinhibited kinase domain of CaMKII and SAXS analysis of the holoenzyme. *Cell* 123:849 – 860.
7. Thaler, C., S. V. Koushik, H. L. Puhl III, P. S. Blank, and S. S. Vogel, 2009. Structural rearrangement of CaMKII α catalytic domains encodes activation. *PNAS* 106:6369 – 6374.
8. Linse, S., A. Helmersson, and S. Forsén, 1991. Calcium binding to calmodulin and its globular domains. *J. Biol. Chem.* 266:8050 – 8054.
9. Meyer, T., P. I. Hanson, L. Stryer, and H. Schulman, 1992. Calmodulin trapping by calcium-calmodulin-dependent protein kinase. *Science* 256:1199 – 1202.
10. Gaertner, T. R., S. J. Kolodziej, D. Wang, R. Kobayashi, J. M. Koomen, J. K. Stoops, and M. N. Waxham, 2004. Comparative analyses of the three-dimensional structures and enzymatic properties of α , β , γ , and δ isoforms of Ca^{2+} -calmodulin-dependent protein kinase II. *J. Biol. Chem.* 279:12484 – 12494.
11. Lengyel, I., S. Fieuw-Makaroff, A. L. Hall, A. T. R. Sim, J. A. P. Rostas, and P. R. Dunkley, 2000. Modulation of the phosphorylation and activity of calcium/calmodulin-dependent protein kinase II by zinc. *J. Neurochem.* 75:594 – 605.
12. Colbran, R. J., 1993. Inactivation of Ca^{2+} /calmodulin-dependent protein kinase II by basal autophosphorylation. *J. Biol. Chem.* 268:7163 – 7170.

13. Endo, S., X. Zhou, J. Connor, B. Wang, and S. Shenolikar, 1996. Multiple structural elements define the specificity of recombinant human inhibitor-1 as a protein phosphatase-1 inhibitor. *Biochemistry* 35:5220 – 5228.
14. Graupner, M., and N. Brunel, 2007. STDP in a bistable synapse model based on CaMKII and associated signaling pathways. *PLoS Comput. Biol.* 3:e221.